Solar Energy Advances 5 (2025) 100083

Contents lists available at ScienceDirect

Solar Energy Advances

journal homepage: www.elsevier.com/locate/seja

A quality control scheme for solar irradiance measurements on facades in urban environments

Nesrin Irmak Köker [a,*], Martina Giorio [a], Gabriele Lobaccaro [a], Gilles Desthieux [b], Peter Gallinelli [b], Bjørn Petter Jelle [a], Mattia Manni [a]

[a] Department of Civil and Environmental Engineering, Faculty of Engineering, Norwegian University of Science and Technology (NTNU), 7491 Trondheim, Norway
[b] Haute école du paysage d'ingénierie et d'architecture de Genève, (HEPIA), University of Applied Sciences and Arts Western Switzerland (HES-SO), 1202 Geneve, Switzerland

ARTICLE INFO

Keywords:
Global tilted irradiance
Solar radiation
Data quality control
Building façade
Shadow detection
Urban monitoring

ABSTRACT

The increasing prominence of digital tools for city-scale solar analysis emphasizes the need for validation methodologies, which include urban environmental monitoring and data quality control. This study addresses this gap by introducing a quality control scheme for solar irradiance measurements, using a typical street canyon in Geneva (Switzerland) as a case study. The developed quality control scheme is replicable and effectively addresses challenges posed by the built environment, distinguishing it from existing methods that mostly apply to measurements from unobstructed sensors. The experimental data used in this study were retrieved from the monitoring system installed on two opposing facades of the street canyon case study, as well as a nearby weather station. Measurements were recorded from December 22nd, 2022, to December 19th, 2023, at a one-minute time resolution. Five quality checks – nighttime check, range limit tests, precipitation check, shadow detection, and consistency check - were defined to identify the potential flaws and disturbances in the dataset so that these data points could be flagged accordingly. The results consist of reliable solar irradiance data over one year, which can be used in the future for validating a new component for modeling façade solar potential within the Grand Geneva Area Solar Cadaster.

1. Introduction

The green energy transition towards a decarbonized society critically depends on the optimal utilization of renewable energy sources (RES) [1]. However, the growing urban population and increasing urban density [2] make it more challenging to fully and optimally exploit RES within urban environments. This highlights the need for adequate tools to support urban planners and designers toward a more sustainable built environment while increasing social awareness, stakeholder engagement, and citizen participation in the green energy transition process [3].

To address these challenges, city-scale solar web platforms like solar maps and solar cadasters have been developed over the last decade [4–6]. Such platforms consist of simplified simulation tools that can be accessed by various users to explore the solar energy potential at multiple scales, ranging from building to district and city scale. The numerical outputs consist of solar resource data for the early-stage urban planning and design of solar installations in urban environments. The information delivered by solar web platforms also allows for economical assessment, including the analysis of costs, savings, and payback time. In addition to utilization for photovoltaics and building integrated photovoltaics applications in urban environments, the development of such solar irradiance simulation tools and corresponding validation methodologies may also be used for miscellaneous other purposes such as exploitation of the solar radiation in daylight and smart windows applications.

Despite the potential of these tools, there is a lack of knowledge about their accuracy and reliability. These can be evaluated, among other methods, by interviewing users or experimentally validating the results. Regarding solar potential estimations on urban surfaces (i.e., roofs, facades, and terrain), solar web platforms have usually been assumed to be accurate since the solar models exploited in their simulation engines are widely applied – and validated in some cases – in the literature. However, in complex urban environments, where facades are considered alongside roofs and where miscellaneous obstructions and varying shadow conditions prevail, achieving satisfactory accuracy and reliability in solar irradiance simulations becomes significantly more

* Corresponding author.
E-mail address: nesrin.i.koker@ntnu.no (N.I. Köker).

https://doi.org/10.1016/j.seja.2024.100083
Received 31 July 2024; Received in revised form 3 December 2024; Accepted 7 December 2024
Available online 7 December 2024

Abbreviations Nomenclatures

Variables

BNI	Beam normal irradiance [W/m^2]
DHI	Diffuse horizontal irradiance [W/m^2]
GHI	Global horizontal irradiance [W/m^2]
GTI	Global tilted irradiance [W/m^2]
H	Height [m]
k_{csi}	Clear sky index [unitless]
RH	Relative humidity [%]
R^2	Coefficient of determination [unitless]
T	Temperature [°C]
W	Width [m]

Subscripts

air	Air
cons	Related to the consistency check
csky	Clear sky
night	Related to the nighttime check
prec	Related to the precipitation check
shad	Related to the shadow detection
range	Related to the range limit tests

Acronyms

BSRN	Baseline surface radiation network
CAMS	Copernicus Atmosphere Monitoring Service
HEPIA	Haute école du paysage, d'ingénierie et d'architecture de Genève
LIDAR	Laser imaging, detection and ranging
NE	Northeast-facing
QC	Quality check
QCS	Quality control scheme
QF	Quality flag
RES	Renewable energy sources
SW	Southwest-facing
UC	Urban canyon
WMO	World Meteorological Organization

Greek letters

α	Angle of incidence of sun rays [°]
θ	Solar zenith [°]
γ	Solar azimuth [°]
ε	Solar elevation [°]

challenging in relation to complex urban phenomena, such as shadowing, inter-building solar reflections from the urban surrounding [7]. In-depth investigations into the performances of these tools as well as of the errors associated with their estimations are currently lacking and should be prioritized. In this regard, the Grand Geneva Area Solar Cadaster, which presents the solar potential of building roofs through the Geoportail (Geneva Information System - SITG) and a web platform application,[1] is exemplary. This solar cadaster implements advanced spatial modeling including (i) transposition of solar irradiance data onto inclined surfaces, (ii) hourly shading based on laser imaging, detection and ranging (LIDAR) data, and a digital surface model of the built environment, and (iii) hourly, monthly, and annual solar irradiation estimations [8,9]. To integrate the building facades into the analyzed geometry, a simplified approach based on radiosity was proposed and applied to the calculation of large urban areas, with a specific focus on the reflection component [10]. This approach was found to provide solar irradiance estimations like existing radiosity approaches, usually applied to small-scale calculations [11]. However, there is a need to go beyond inter-model comparisons and perform experimental validation of such methods with solar irradiance measurements from real-scale urban environments.

2. Background

2.1. State-of-the-art quality control schemes

Experimental measurements are essential for validation studies, offering critical data for evaluating the accuracy and reliability of predictive models. However, various factors can introduce errors in these measurements, potentially compromising the overall reliability of the validation study. To guarantee the integrity and consistency of the measurement dataset, multiple quality control schemes (QCSs) and tests have been proposed in the literature; however, such schemes were mostly developed for weather stations and other sensors that are not influenced by the surroundings (i.e., unobstructed). In the context of solar irradiance, such QCSs typically focus on global horizontal irradiance (GHI), beam normal irradiance (BNI), and diffuse horizontal irradiance (DHI), with global tilted irradiance (GTI) being less commonly addressed.

The QCS proposed by the Baseline Surface Radiation Network (BSRN) [12] and further improved by Roesch et al. [13] is among the most adopted QCS since it provides a list of physical ranges for the diverse solar variables (e.g. GHI, BNI, DHI). These tests (also known as "range limit tests") are integrated into the majority of the current QCSs [14–17]. In particular, Geiger et al. [18] implemented a web service for the quality control of GHI and tested it with data from the World Meteorological Organization (WMO) network. Measurements were verified against reference values calculated from clear sky irradiance (GHI_{csky}) and extraterrestrial irradiance (GHI_{extra}). In the study by Long and Shi [17], an automated algorithm for the quality check (QC) of surface radiation measurements was presented. Besides the physically possible limits from the BSRN's QCS, user-configurable limits based on climatological data to detect erroneous values were proposed. A quasi-automated QCS was developed by Journée et al. [19] for the Royal Meteorological Institute of Belgium (RMIB) solar measurements network. The steps of the QCS involved (i) physical threshold tests, (ii) step tests to detect abrupt sensor issues, (iii) persistence tests, (iv) quality envelope tests and (v) sunshine tests to validate and accurately report clear sky periods. In this study, the quality envelope tests were employed using historical data to identify outliers, while spatial consistency tests were applied to ensure uniformity across proximate measurement sites. Moreover, a data-filling procedure involving empirical solar models was proposed to provide users with solar irradiance estimations that could replace the missing or inaccurate data points in the dataset.

Perez-Astudillo et al. [20] further advanced the BSRN's QCS by introducing 19 tests, including QCs for physically plausible values, consistency among the diverse irradiance components (i.e., GHI, DHI, and BNI), and comparisons against clear sky models designed to automatically identify incorrect measurements. The validation against data from Doha (Qatar) and Dar Es Salaam (Tanzania) demonstrated that the new protocols could detect errors overlooked by the BSRN's QCS. Conversely, the QCS proposed by Yang et al. [16] focused on aggregated data to statistically identify cloud enhancement events. In addition to ground-based measurements of solar variables, supplementary satellite-driven data was used. Urraca et al. [21] introduced an open-access web platform for QC of solar irradiance data, providing both visual and numerical quality flags (QFs) to identify discrepancies. The proposed method named the Bias-based Quality Control method detects

[1] apps.sitg-lab.ch/solaire (Accessed on 29/07/2024)

low-magnitude measuring errors that traditional QCSs often overlook. However, it requires a dense network of ground stations to guarantee enough historical data in a large spatial domain for statistically identifying the anomalies.

Finally, Lorenz developed a QCS for a high-resolution solar irradiance measurement network in southern Germany, comprising 40 meteorological stations [15]. The QCS includes physical range limits for irradiance and temperature measurements; detection of anomalies such as snow, ice, and water on pyranometers; sensor consistency tests; and manual flagging for persistent issues. The study further advanced the BSRN's QCS by implementing new tests that utilize machine learning techniques to detect issues concerning shading and orientation of the sensors. Unlike other studies, Lorenz's QCS was also applied to GTI, as their network included pyranometers facing all four cardinal directions. However, it is worth noting that these measurement stations were only obstructed by terrain.

The analysis of the state-of-the-art QCSs highlighted (i) the scarcity of studies addressing GTI as well as (ii) the lack of a QCS for application in urban environments. In such settings, solar irradiance measurements can be significantly influenced by factors such as shadows from surrounding buildings, mutual shading between structures, and ground reflections. These urban-specific phenomena can cause unique distortions and anomalies in the datasets that traditional QCSs may not properly identify. Consequently, there is a pressing need to develop specialized QCSs tailored specifically for urban environments.

2.2. Motivation and objectives of the study

The present study aims to develop a QCS taking into account GTI in urban settings, using on-site measurements collected at multiple levels on two opposing building facades within a street canyon in Geneva (Switzerland) as a case study. This research advances the state-of-the-art by addressing the research gaps identified in Section 2.1. Moreover, the study introduces a QCS specifically designed for urban environments, with a particular focus on the detection shadows cast by surrounding buildings and the verification of pyranometer alignment.

The proposed workflow comprises intra-sensor and inter-sensor QCs, incorporating both data handling and data processing techniques. Intra-sensor QCs explore data acquired from each sensor, while the inter-sensor QCs analyze data from multiple sensors. Furthermore, the proposed QCS can function as an operational tool to identify and select the portions of datasets most relevant for investigating the various factors that influence measurement reliability. Indeed, labeling the data points with diverse QFs allows the user to better manage the datasets, controlling the overall level of data quality according to their specific needs. For example, some QCs enable flagging data points as "potentially inaccurate" when the solar elevation is below 5° from the horizon. However, a researcher interested in studying the influence of horizon brightening (i.e., diffuse irradiance from the horizon band) on pyranometer readings might use this flag to selectively filter and analyze this group of data points.

In the following sections, we present the measurement setup and system calibration (Section 3), the methodology for data QCS (Section 4), the results and discussion (Section 5), and the conclusions and future works (Section 6). Section 3 presents the configuration of the monitoring apparatus (Section 3.1), the preliminary pyranometer calibration (Section 3.2), and an overview of the acquired datasets (Section 3.3). Section 4 focuses on the study workflow and the structure of the QCS (Section 4.1), the intra-sensor QCs (Section 4.2), the inter-sensor QC, and the shadow detection method (Section 4.3). Then, the results are presented along with discussions in Section 5, providing insights into the preparatory phase (Section 5.1), the intra-sensor QCs (Section 5.2), the inter-sensor QC (Section 5.3), the assigned QFs (Section 5.4), validation, and potential improvements of the shadow detection algorithm (Section 5.5), and the limitations of the study (Section 5.6). The study concludes with a summary of the main findings and an overview of potential future developments (Section 6).

3. Measurement setup and system calibration

3.1. Monitoring system configuration

The experimental case study setup is located at Rue des Grottes (Fig. 1), a street in the center of Geneva (Switzerland) classified as a street canyon (i.e., two opposite lines of buildings developing along a linear street). The height (H) of the buildings along Rue des Grottes is approximately 13 m, which is also the width (W) of the street. Therefore, the aspect ratio of the street (also known as the height-to-width ratio) is 1 (i.e., $H/W = 1$). The typical facade color is beige, reflecting some solar radiation onto the opposite side of the street and toward the facades across from it. The street has a standard grey surface, while the sidewalks are made of cement.

Rue des Grottes is aligned along a southeast-to-northwest axis. Consequently, the streetscape faces southwest (surface azimuth angle is 226°) and northeast (surface azimuth angle is 33°). This orientation results in the southwest-facing (SW) façade receiving solar radiation primarily in the afternoon and early in the evening, while the northeast-facing (NE) façade receives solar radiation primarily in the morning. The sky view of a building frontage is reduced by the fabrics on the opposite side that obstruct the path of sun rays when the sun is low above the horizon. Additionally, solar inter-building reflections can take place within Rue des Grottes, resulting in the increment of the solar energy potential of the different urban surfaces. The measurement setup was designed to investigate the complex urban phenomena (e.g., shadowing, solar mutual inter-building, and ground reflections) that characterize a street canyon and the urban environment in general. Six (6) Kipp & Zonen CM-11 pyranometers were attached to the facades of two opposite 4-story buildings at three different heights, ranging from the 1st (circa 4 m above the ground) to the 3rd floor (circa 10 m above the ground), oriented normally to the façade (Fig. 2).

This measurement setup allows the collection of data concerning the spatial variation of the solar energy potential along the building elevation. Any group of three pyranometers installed on the same façade was powered by a solar module, which was also connected to a data logger for local data storage. The pyranometers measure GTI with a one-minute time resolution. The sensor layout is completed by a weather station mounted on the rooftop of the main building of the Haute école du paysage, d'ingénierie et d'architecture de Genève (HEPIA), located approximately 300 m from Rue des Grottes. The weather station measures the GHI and DHI through two Kipp & Zonen CM-11 pyranometers mounted on a solar tracker; the ambient average temperature (T_{air}) and the relative humidity (RH) using the integrated Metpack (R); and the total rainfall using the Precis (R) mechanical rain gauge. The sensors of the weather station are connected to a central common Campbel Scientific CR3000 (R) datalogger. Similar to the monitoring system on Rue des Grottes, observations are collected with a one-minute time resolution.

The monitoring campaign was performed between the 22nd of December 2022 and the 19th of December 2023, resulting in the collection of 522 720 data points for each sensor.

3.2. Preliminary calibration of the pyranometers

A preliminary calibration was performed to compare the pyranometers' readings and detect possible malfunctions of the equipment before the monitoring campaign. Therefore, the six sensors were positioned side by side on a horizontal surface, situated near the reference pyranometer of the HEPIA weather station, which is equipped with a factory-calibrated CM-11 pyranometer. A short period of three consecutive days in September 2022 was selected before starting the monitoring campaign. Linear regression analyses conducted between the readings of the pyranometers and the reference pyranometer at the

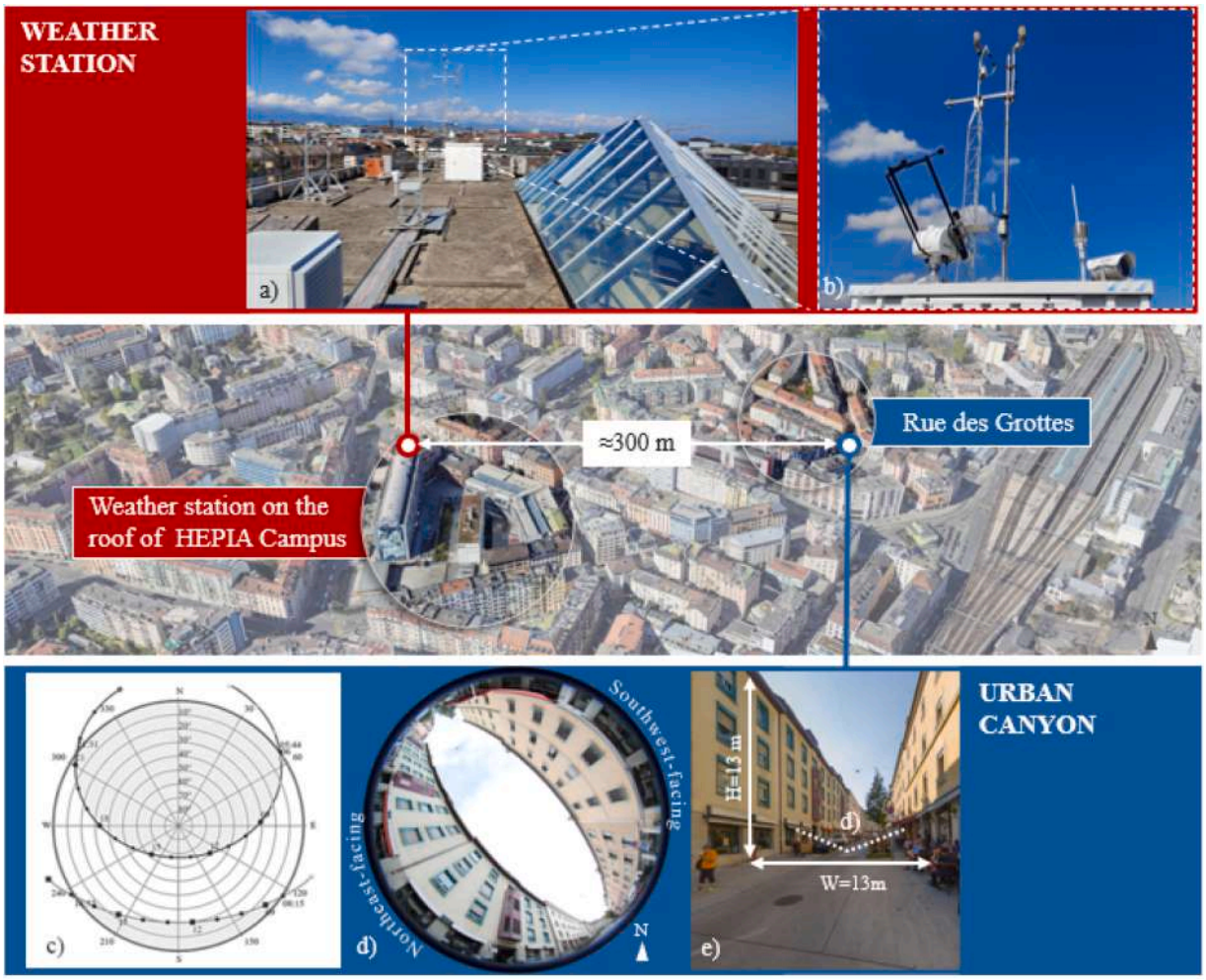

Fig. 1. Location of the weather station (in red) and the urban canyon of Rue des Grottes (in blue): a) the rooftop of the HEPIA campus where the weather station is installed; b) the zoomed-in view of the weather station; c) the north-south (N-S) oriented sun path of Geneva; d) the SW-NE oriented fisheye image; and e) the street view of Rue des Grottes.

HEPIA weather station demonstrated a strong overall correlation, with the coefficient of determination (R^2) consistently exceeding 0.980. Similarly, a robust correlation was observed among the readings from the six pyranometers (see Fig. 3). The fit function was further used to correct the readings from the pyranometers, allowing for an overall R^2 close to 0.999.

3.3. Acquired datasets

In this section, the datasets used in this study are presented. The main dataset includes sensor readings from the HEPIA weather station (Fig. 4) and the pyranometers on the building facades (Fig. 5). The auxiliary dataset includes all the additional variables (i.e., GHI_{csky}, solar zenith, azimuth, elevation, and angle of incidence) that are needed to perform the QCs. The GHI_{csky} values were retrieved from the Copernicus Atmosphere Monitoring Service (CAMS) database.[2] These amounts consist of satellite observations with a one-minute time resolution, covering the same time interval as the monitoring campaign. Additionally, the *aoi*, and *get_solarposition* functions from the *irradiance* module of the *pvlib* library in Python were utilized to calculate the angle of incidence of the sun rays (α), the solar zenith (θ), the solar azimuth (γ), and the solar elevation (ε).

4. Methodology for data quality control scheme

4.1. Workflow of the study

To ensure the accuracy and reliability of solar irradiance measurements, a structured workflow (Fig. 6) consisting of four steps was developed: (i) the preparatory phase, (ii) the intra-sensor QCs, (iii) the inter-sensor QC, and (iv) the combination of the QFs. This workflow is fully automated and does not require any manual checks or flagging (i.e., assignation of a QF to a data point for describing its level of reliability or other features) of data points.

The workflow starts with *Step 1 - Preparatory phase*, during which the time synchronization across all sensor readings and the auxiliary dataset was verified. Additionally, the alignment of the pyranometers was checked. For the synchronization check, the time resolution was first examined to ensure that the frequency of data acquisition – one minute in this study – was the same across the different sensors. Then, the extremes of the time interval (from the 22nd of December 2022 to the 19th of December 2023) of the observations are verified to be synchronized.

[2] Inness, A, Ades, M, Agustí-Panareda, A, Barré, J, Benedictow, A, Blechschmidt, A, Dominguez, J, Engelen, R, Eskes, H, Flemming, J, Huijnen, V, Jones, L, Kipling, Z, Massart, S, Parrington, M, Peuch, V-H, Razinger M, Remy, S, Schulz, M and Suttie, M (2019): CAMS global reanalysis (EAC4). Copernicus Atmosphere Monitoring Service (CAMS) Atmosphere Data Store (ADS). (Accessed on 29/07/2024), ads.atmosphere.copernicus.eu/cdsapp#!/dataset/cams-global-reanalysis-eac4?tab=overview

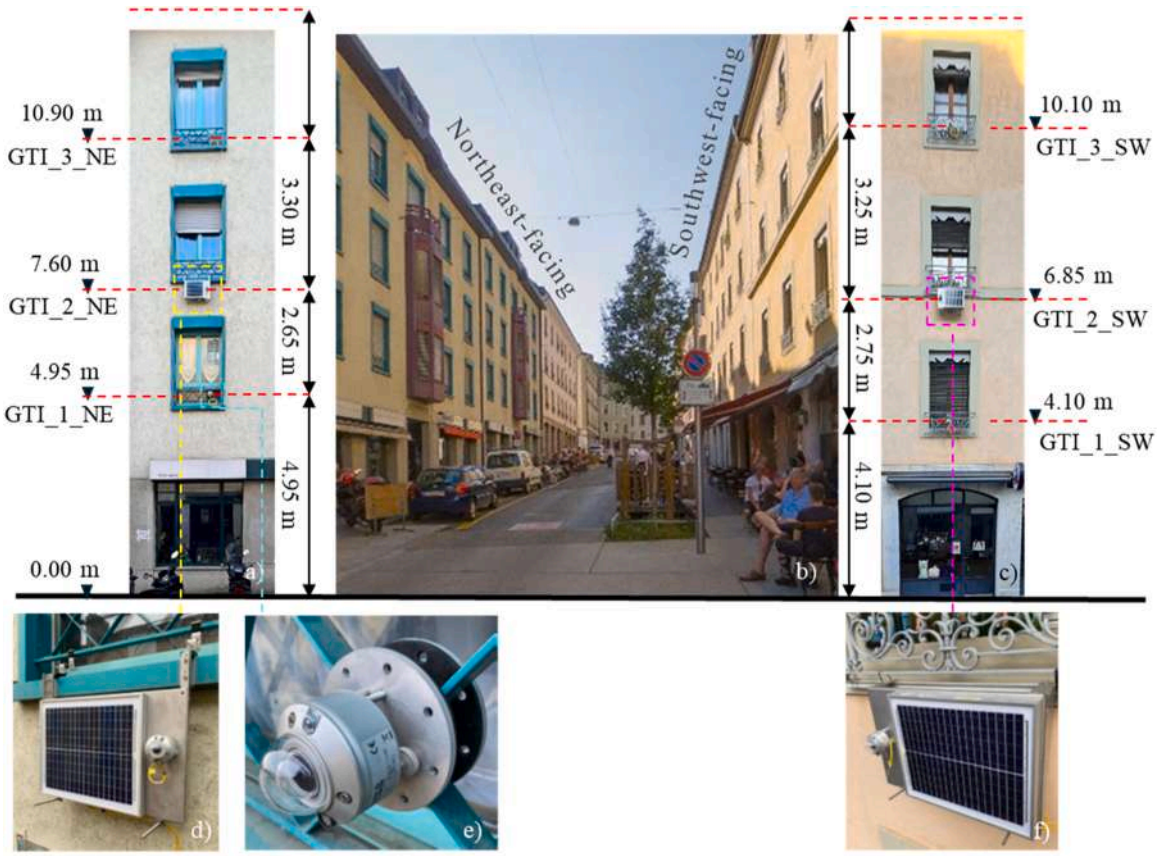

Fig. 2. Monitoring in the urban canyon Rue des Grottes: pyranometer placements on the a) northeast-facing facade and c) southwest-facing facade; b) street view of the urban canyon; d) and f) autonomous solar power supply, battery and data logger Campbel Scientific CR1000 (R), fixed to the railing; and e) pyranometer.

The alignment check aims to determine whether the sensors were aligned along the same direction or if something occurred that altered their alignment (e.g., something hit one of the sensors). This test is conducted for a specific portion of the dataset rather than for each data point. In the alignment check, the uniformity of the orientations of the three pyranometers installed on the same facade is verified. This check is performed for both facades, considering the corresponding clear sky index (k_{csi}) which is the ratio of GHI to GHI_{csky}. The check was performed on data points with a very high daily average k_{csi} value ($k_{csi} > 0.90$) representing minimum cloud coverage throughout the day and for periods when pyranometers were simultaneously unobstructed by shadows created by the surroundings. A linear regression analysis is performed on the measurements from each of the three pyranometers installed on the same façade to analyze if the recorded values are linearly correlated (i.e., measurements from a pyranometer can be used to predict solar irradiance observed by another pyranometer on the same façade) and follow a similar trend (i.e., solar irradiance peaks at the same time in the observations from different pyranometers) for the indicated time interval.

Step 2 - Intra-sensor QCs include all the tests that were conducted on readings from a single sensor (i.e., data from different sensors were not compared). The four (4) QCs consist of (i) nighttime check, (ii) range limit tests, (iii) precipitation check, and (iv) shadow detection. During the nighttime check, the sunrise and sunset times were used to identify and flag data points recorded during the night hours ($QF_{night} = 1$). Daytime data points were considered to pass the test ($QF_{night} = 0$). The range limit tests permitted to flag GHI and GTI measurements that fall outside the pre-defined physical range limits (see Section 4.2 for the determination of the physical range limits). In this case, a QF_{range} of 0 was assigned to solar irradiance measurements within the acceptable range, while a QF_{range} value between 2 and 3 was assigned depending on the likelihood that the measurement was erroneous. A QF_{range} of 1 indicates that the test could not be performed. The precipitation readings collected by the HEPIA weather station were analyzed in the precipitation check, giving a QF_{prec} of 1 whenever a precipitation event occurred. Afterward, in the shadow detection assessment, the urban surroundings (e.g., buildings, architectural elements, light poles) causing the periodic shading of pyranometers were accounted for. Shadows cast on sensors by permanent obstructions were empirically identified for all pyranometers (see Section 4.3) and data points from façade pyranometers were categorized into "*unshaded*" ($QF_{shad} = 0$) or "*shaded*" ($QF_{shad} = 1$).

Step 3 - Inter-sensor QCs concerns the QCs that assessed data quality by comparing data from multiple sensors. In the present study, only the consistency check was considered for this QC category. During the consistency check, the uniformity of the different time series was verified, identifying the missing data points across measurements from all sensors. Whenever a missing value was identified, the corresponding timestamp (i.e., time of the measurement) was flagged with a $QF_{cons} = 1$. Otherwise, a $QF_{cons} = 0$ was associated with the measurement. Timestamps with a $QF_{cons} = 1$ provided incomplete information, therefore, they were considered inaccurate.

Finally, during the *Step 4 - QF combination*, the QFs assigned during *Step 2* and *Step 3* (and summarized in Table 1), were integrated into a single dataset. This combined dataset offers a comprehensive synthesis of the QFs, highlighting the reliability level of each measurement.

4.2. Intra-sensor quality checks

Step 2 - Intra-sensor QCs includes the nighttime check, range limit tests, precipitation check, and shadow detection.

The **nighttime check** aims at flagging the nighttime data points to

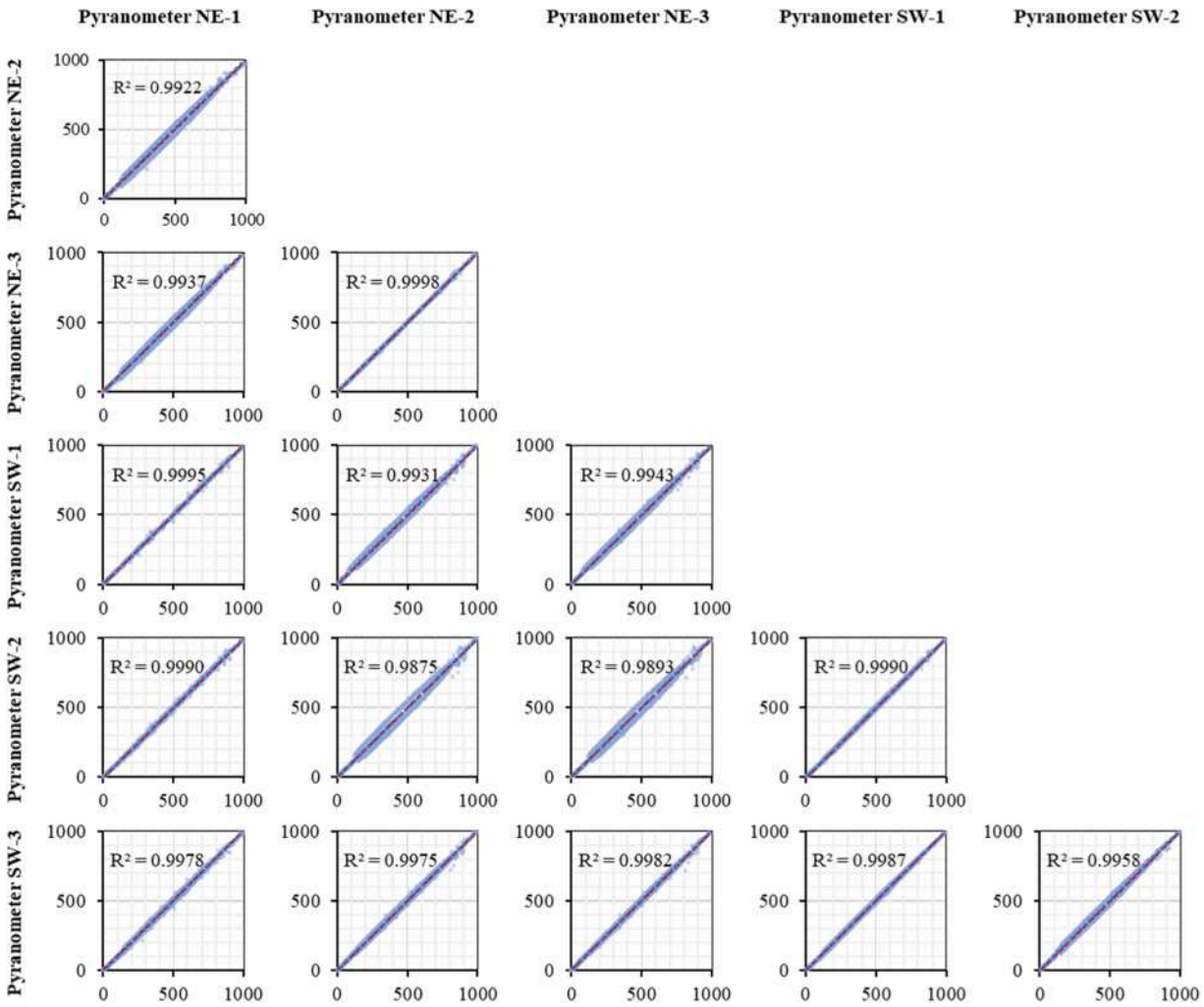

Fig. 3. Pre-calibration linear regression analysis between the pyranometer readings.

avoid confusing the low irradiance amounts measured during the night because of streetlights or erroneous readings with the low irradiance amounts recorded during extremely overcast days. The *get_sun_rise_set_transit* function from the Python *pvlib* library was used to calculate the sunrise and sunset times for each day based on the geographical coordinates (latitude and longitude) of the case study location. All data points captured during nighttime (i.e., after sunset time and before sunrise time) were flagged with the value 1, while those recorded during daytime (i.e., between sunrise time and sunset time) were flagged with the value 0.

The **range limit tests** moved from the calculation of the physical upper and lower limits for both GHI and GTI to the flagging of those measurements that exceeded such limits. These range limits, representing the maximum and minimum values that measurements can physically reach, are based on extrema and determined by extraterrestrial irradiance (GHI_{extra}) and solar zenith angle (θ). Table 2 presents the range limits and their corresponding flag values. For the GHI upper limits, the upper envelope function used by Espinar et al. [22] was applied to identify rare ($QF_{range} = 2$) and extreme solar irradiance values ($QF_{range} = 3$). The function to define $QF_{range} = 2$ for GTI in the range limit test and lower limits ($QF_{range} = 3$) for both GHI and GTI was identical to the one proposed by Lorenz et al. [15], as the two case study locations share similar characteristics when it comes to solar irradiance. Additionally, the maximum step change limit suggested by Espinar et al. [22] was used to detect abrupt changes between two consecutive measurements that could indicate erroneous readings or transient environmental conditions not representative of regular solar irradiance patterns (e.g., cloud-enhancement events, instantaneous shadows, and reflections). The QF_{range} ranges from 0 to 3, where 0 indicates that the test was passed, 1 means the test could not be performed, 2 indicates that the measurement was likely to be erroneous and 3 indicates that the measurement was most likely erroneous.

The **precipitation check** permitted the identification of potentially erroneous measurements in correspondence with precipitation events. Rain droplets on pyranometer glass can affect the accuracy of solar irradiance readings by scattering, reflecting, absorbing, or concentrating the solar radiation, ultimately causing inaccurate measurements. Data points that coincide with non-zero total rainfall values were flagged with a value of 1, while the others were flagged with a value of 0.

Finally, the **shadow detection** analysis enabled the empirical identification of the pyranometer readings that were recorded when the sensor was shaded. In particular, the analysis focused on detecting periodic shadows (see Section 4.3 for the definition of "periodic shadows") cast by both neighboring buildings and architectural features of the monitored façades, like overhangs, recessed windows, and parapets. The shadow detection was articulated into four diverse sub-steps. Firstly, the k_{csi} was calculated and used to select measurements taken under exceptionally clear sky conditions ($k_{csi} > 0.75$) so that temporary shadow from clouds was excluded (see Section 4.3.1). Afterward, the dataset was smoothed by filling the excluded data points with moving average smoothing. A clustering technique (Section 4.3.2) was later applied to group data points into "*shaded*" and "*unshaded*" clusters and

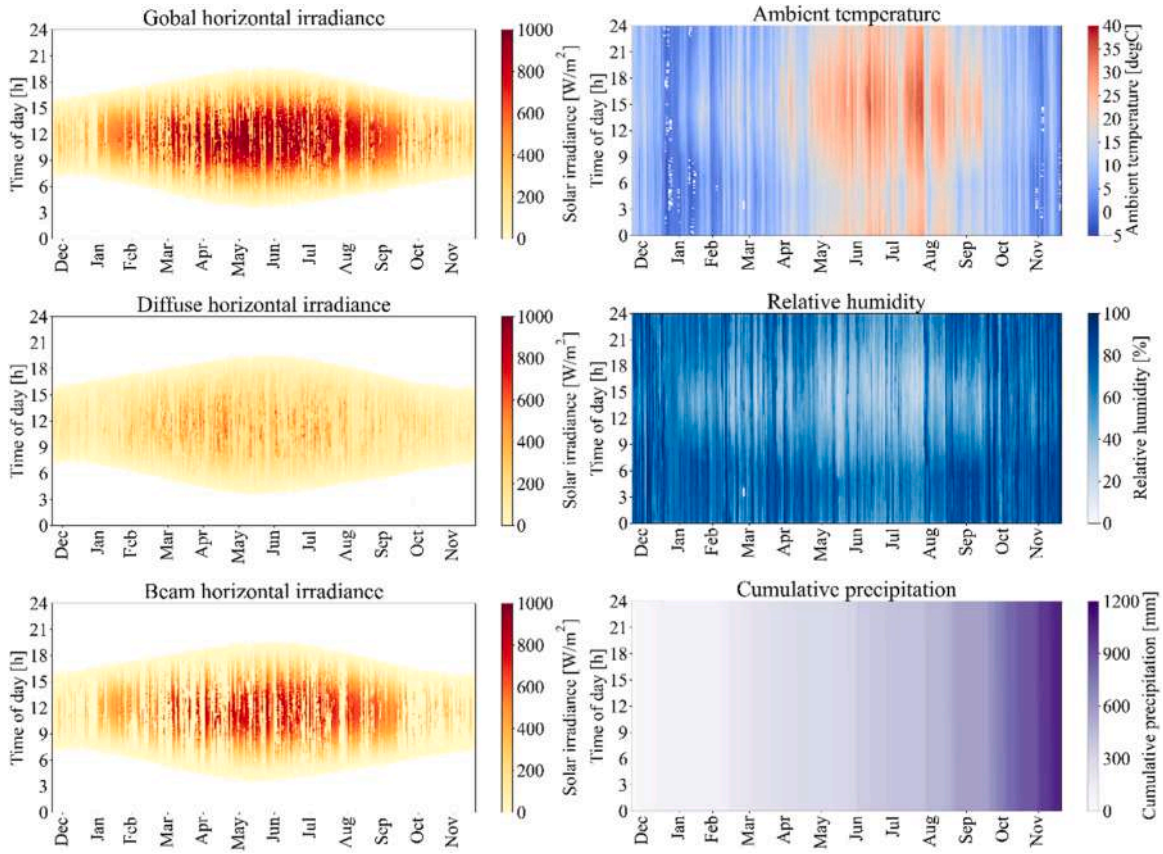

Fig. 4. Global horizontal irradiance, diffuse horizontal irradiance, beam horizontal irradiance, ambient temperature, relative humidity, and precipitation, measured from the HEPIA weather station.

flag them accordingly. Finally, a local outlier detection technique is applied to the created clusters to identify and correct misclassifications by detecting outliers within each group (see Section 4.3.3). The outcomes of the shadow detection and its various sub-steps are detailed in Section 5.2.

4.3. Shadow detection method

This section describes the algorithm developed for detecting periodic shadowing of pyranometers. The proposed methodology is based on and advances the one by Lorenz et al. [15]. Specifically, the newly introduced shadow detection algorithm combines multiple rounds of clustering (clustering cascade) with local outlier detection, as opposed to the single clustering round in Lorenz's method. The clustering cascade is a multi-step process where the same clustering technique is first applied to each pyranometer reading (α and ε are also input parameters). The same clustering technique is then iteratively applied to each cluster again. This process can be repeated until the clusters detected are deemed sufficiently accurate. In this study, a two-step clustering cascade was applied to the pyranometer records to group measurements into "*shaded*" and "*unshaded*" according to their distribution in the α-ε plane (see Fig. 7). Local outlier detection was also integrated into the algorithm to refine the grouping within single clusters. As Lorenz's method was designed for detecting horizon profiles, it lacked accuracy when addressing the higher complexity of a street canyon as the one hereby investigated. While both this study's sensors and those of Lorenz's work were exposed to both temporary shading – caused by transient elements such as clouds or birds – and periodic shading, which results from permanent obstructions like surrounding buildings or horizon profiles (Fig. 7a), the sensors in this study also experienced self-shading effects from the building on which they were mounted. These self-cast shadows are indeed more challenging to detect with Lorenz's method since the shadow profiles can be irregular and coarse, making it necessary to enhance the clustering technique.

4.3.1. Dataset preparation

The preparation of the dataset for the two-step clustering cascade and local outlier detection involved (i) removing all data points corresponding to temporary shading conditions and (ii) filling the resulting gaps, as in [15].

To exclude temporary shadow events related to overcast conditions, the data points with a k_{csi} greater than 0.75 (clear sky conditions) were filtered out. Fig. 7b shows how the remained shadows (i.e., extremely low solar irradiance values) were due to the presence of surroundings. It is worth noting that temporary shadows caused by unpredictable elements, like birds, were not excluded through this process, as these events are independent of sky conditions. However, their occurrence is extremely rare, and their inclusion in the analysis does not compromise the results.

A rolling window smoothing technique (also known as moving average smoothing) was used to smooth the dataset and fill the gaps left after the exclusion of data points with $k_{csi} < 0.75$. This method involves considering a window of measurements (i.e., a group of data points) around an empty data point and substituting such a missing value with the rolling mean of the measurements within the chosen window. In this application, a window of measurements was defined as a group of five (5) data points that are contiguous and distributed vertically within the α-ε plane (same γ value and five different ε values). By applying this smoothing technique, a hybrid and continuous dataset – including both measured and modeled k_{csi} values – was generated (Fig. 7c).

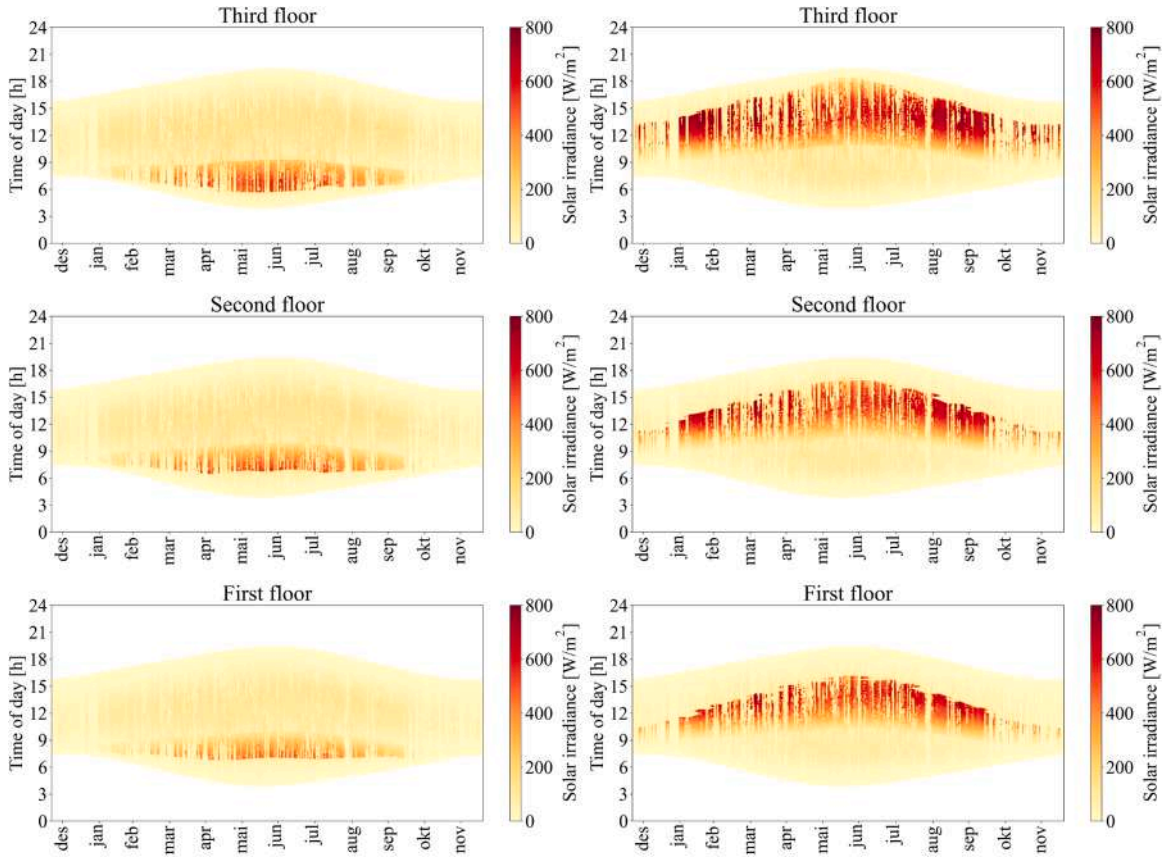

Fig. 5. Global tilted irradiance measured by the pyranometers in Rue des Grottes. On the left, readings from the northeast façade; on the right, readings from the southwest façade.

4.3.2. Clustering cascade

The k-means clustering method was exploited in the two-step clustering cascade to group the measurements into "*shaded*" and "*unshaded*" (i.e., the number of clusters is 2). The k-means clustering is a method that groups data points into a specified number of clusters based on similarity. This similarity is quantified as the distance between each data point and the center of each cluster (i.e., the mean of the cluster). Each data point is assigned to the cluster with the nearest center. The *Kmeans* algorithm from the *sklearn.cluster* module in the Python *scikit* library was used.

Repeating the clustering process was necessary to refine the results since the algorithm, after the first step (Fig. 7d), failed in detecting the shadows cast from the same building façade where the pyranometer is mounted (Fig. 8a). In fact, the second round of k-means clustering, which was only conducted on data points labeled as "*shaded*" (QF_{shad} = 1) after the first clustering, succeeded in differentiating between shading from the surroundings, self-shading (by the building itself), and unobstructed data points (Fig. 8b).

4.3.3. Local outlier detection

The density-based local outlier detection algorithm called *LocalOutlierFactor* from *sklearn.neighbors* module in Python *scikit* library was integrated into the algorithm to detect and correct the outliers located in sparsely populated regions within each cluster. In other words, a data point that has a different label than the neighboring data points is detected as an outlier, and the label is corrected to the other cluster. The comparison of Fig. 8b and Fig. 8c highlights the capability of the local outliers detector to further refine the clustering process.

5. Results and discussion

This section presents the results of the QCS as well as the QFs assigned according to the workflow described in Section 4. Each paragraph focuses on a specific step, discussing potential applications of the results.

5.1. Preparatory phase

Synchronization check. The synchronization check confirmed that all sensor readings and auxiliary datasets were properly aligned. The observations span within the desired time interval with a consistent time resolution of one minute. No discrepancies were found in the synchronization or time resolution.

Alignment check. The results of the regression analysis show significant agreement between the sensors on the same façade for both NE and SW pyranometers (Table 3). The solar irradiance measurements that were used in the regression analysis were collected for four days characterized by extreme clear sky conditions. The measurements for the 5th of June 2023 are presented in Fig. 9, grey areas indicate the periods of simultaneous unobstructed conditions. The outcomes demonstrate that the sensors on the same façade are aligned in the same orientation.

5.2. Intra-sensor quality checks

Nighttime check. The number of data points flagged as nighttime is presented in Table 4. The nighttime QC identifies irrelevant data for solar analyses and makes it easier to detect solar irradiance measurements greater than zero during nighttime hours. Such measurements may result from pyranometers malfunctioning or the influence of artificial lighting, as pyranometers mounted on facades can show sensitivity

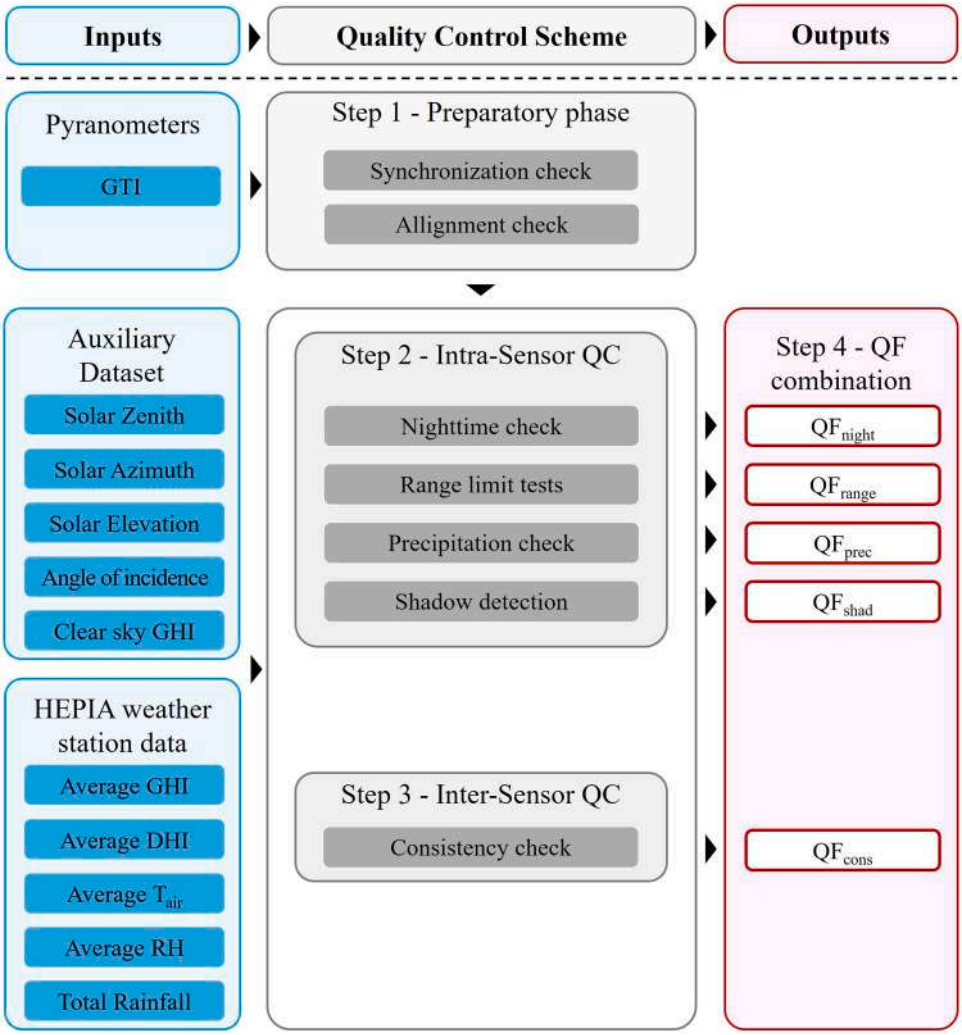

Fig. 6. Proposed workflow overview for the QCs.

Table 1
Overview of the quality flags assigned during each quality check. A short description is provided for each possible flag value.

Quality Flag	Flag Values	Description
QF_{night}	0	Daytime
	1	Nighttime
QF_{range}	0	Safe data (passed the tests)
	1	Tests cannot be performed
	2	Data likely to be disturbed or erroneous
	3	Data most likely to be disturbed or erroneous
QF_{prec}	0	No precipitation
	1	Precipitation event
QF_{shad}	0	No periodic shadowing
	1	Periodic shadowing present
QF_{cons}	0	No missing value
	1	Missing value in one of the data points

to streetlights. In this regard, pyranometer readings greater than zero occurred during the nighttime, particularly on the second floor (Fig. 10).

It is worth noting that several non-zero values can be observed around sunset and sunrise hours. These measurements can be primarily attributed to the diffuse solar irradiance coming from the horizon band (during twilight hours) rather than artificial lighting. The algorithm used to calculate sunset and sunrise hours incorporates a coefficient to consider the atmospheric fraction, but this does not fully account for atmospheric scattering during twilight hours. This limitation is more evident in the NE façade as well as in the upper floors, which are characterized by a higher sky view factor if compared to the lower ones (Fig. 10). The visual inspection of the nighttime data points suggests that the calculation method for sunset and sunrise hours requires further improvement to account for atmospheric scattering during twilight periods.

Range limit test. In Table 5 the number of data points that were

Table 2
The QF_{range} values for the range limit tests of the GHI and GTI.

	Flag Values	GHI	GTI
Upper Limit	2	$1.2\ GHI_{extra}\cos(\theta) + 50\ W/m^2$	$0.9\ GHI_{extra}\cos(\alpha)^{1.2} + 300\ W/m^2$
	3	$\min(1.2\ GHI_{extra};\ 1.5\ GHI_{extra}\cos(\theta)^{1.2} + 100\ W/m^2)$	-
Lower Limit	3	for $\theta \leq 75°$, $0.01\ GHI_{extra}\cos(\theta)$ for $\theta > 75°$, 0	
Max. Step	3	$1000\ W/m^2$	

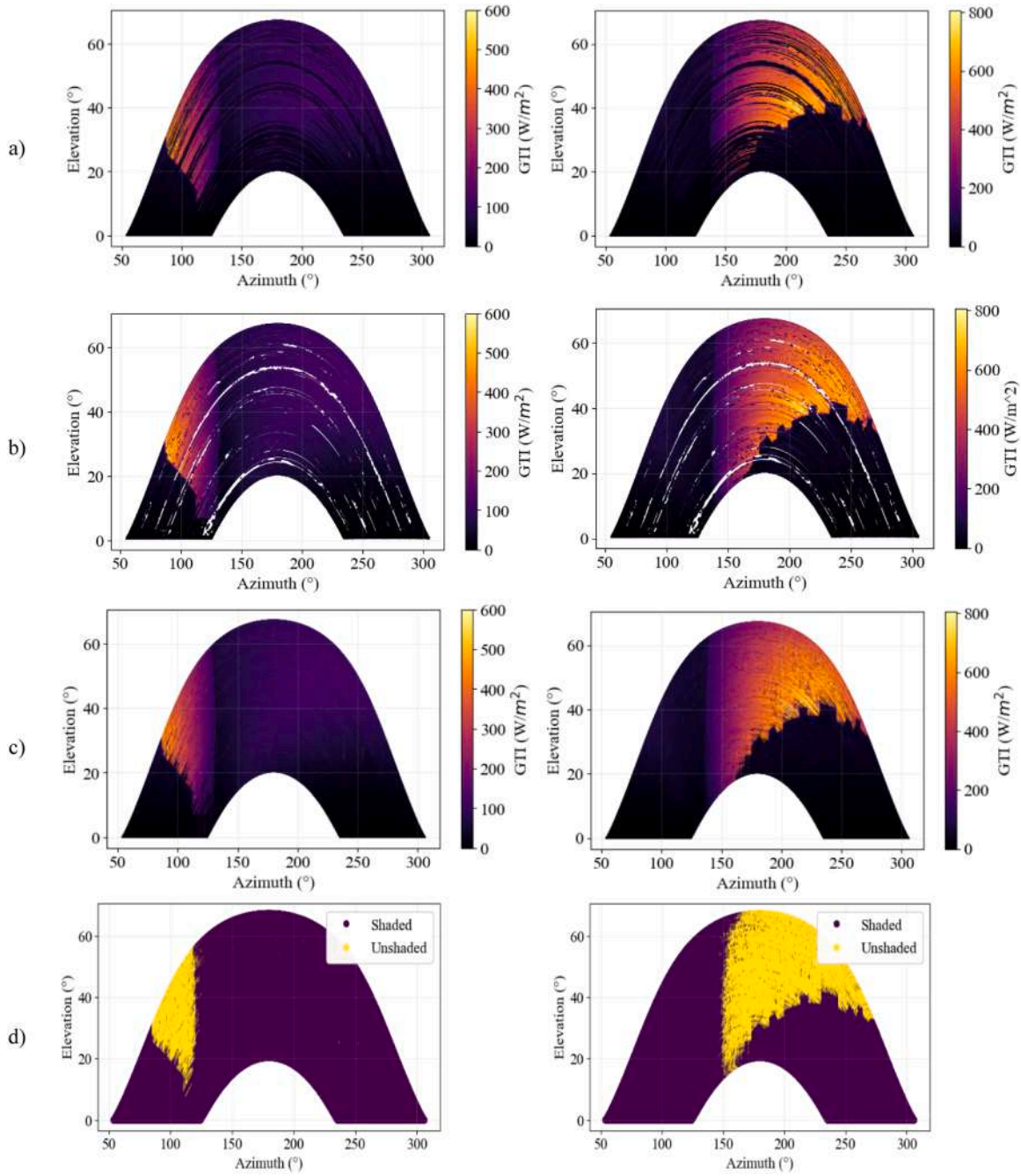

Fig. 7. a). Pyranometer measurements installed on the first floors of the two opposite facades; b) Pyranometer measurements installed on the first floors of the two opposite facades after exclusion of overcast sky conditions; c) Pyranometer measurements installed on the first floors of the two opposite facades after smoothing technique; d) Results of the first round of clustering of observations from the first floors of the two opposite facades. For all measurements: on the left, the NE façade; and on the right, the SW façade.

flagged based on the physical range limits are reported. The application of these limits allowed the identification of the extreme values that provide the basis for further investigation of the causes of the anomalies. Such anomalies could range from sensor errors to sudden or short-term changes in environmental conditions (e.g., temporary shading, solar irradiance reflection on the sensor).

None of the GHI measurements from the HEPIA weather station exceeded the upper range limit, and only 152 data points (accounting for 0.056% of the entire dataset) fell below the lower range limit. Additionally, 0.248% of the GHI measurements could not be tested due to missing values. For façade-mounted pyranometers, the values were significantly below the upper limit, except for a total of 22 outliers (see Table 5). Conversely, a considerable number of data points were flagged below the lower limits, which, upon further analysis, were attributed to extremely overcast sky conditions (with maximum $k_{csi} < 0.22$). Moreover, these data points were recorded on the same days for all pyranometers, hence supporting the correlation between lower limit flags and sky conditions. Notably, no data points were flagged during the maximum step change check.

Precipitation check. The number of data points that were flagged for precipitation events is presented in Table 6. A total of 2129 (0.8%) data points were flagged among the daytime measurements ($QF_{night} = 0$). These can represent the basis for further studies about the influence of precipitation on solar irradiance measurements. For example, the

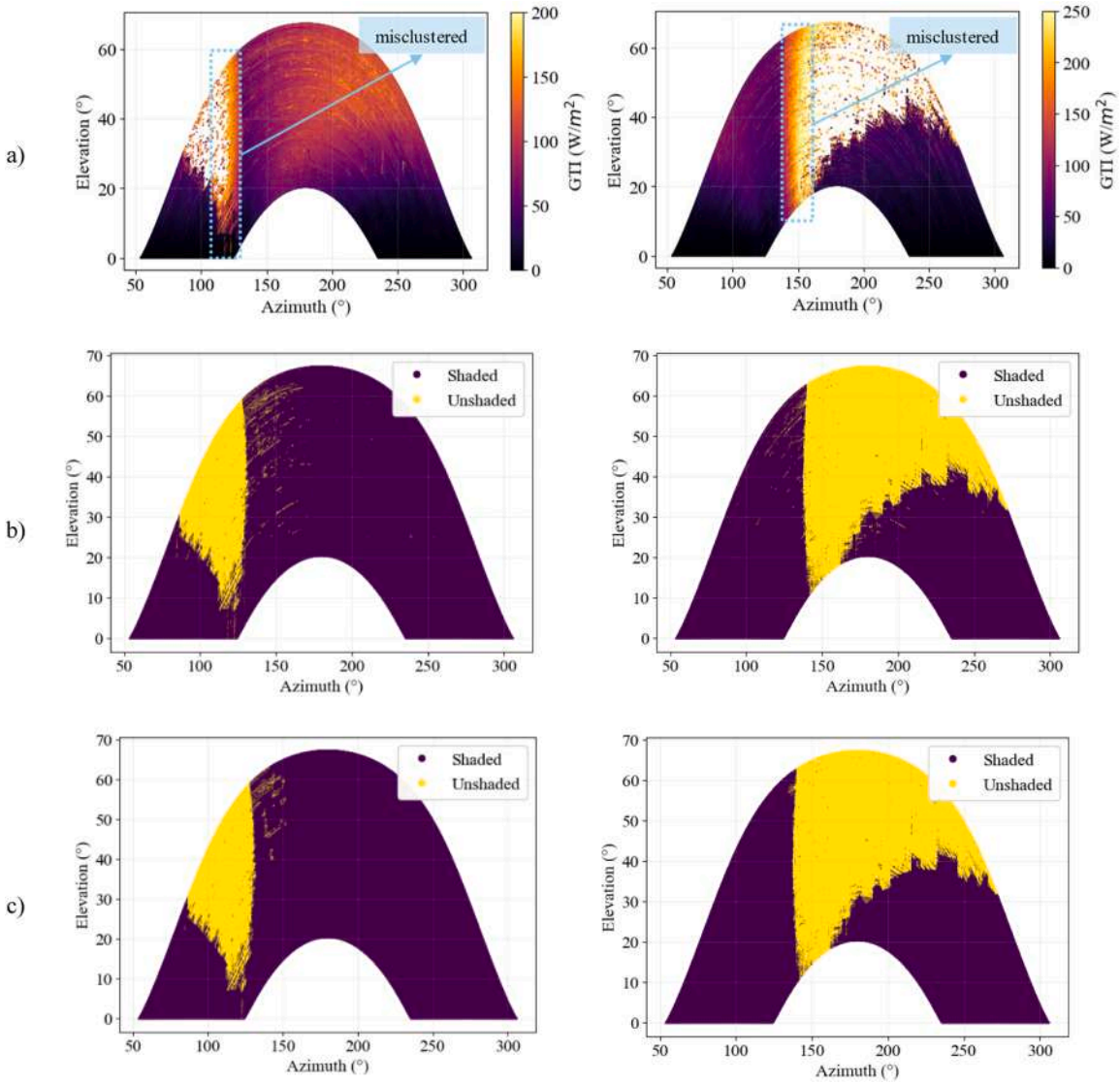

Fig. 8. a). Pyranometer measurements installed on the first floors of the two opposite facades excluding data points flagged as unshaded in the first round of clustering, misclustered data points are highlighted; b) Results of the second-round cluster cascade of the first floors of the two opposite facades; c) Final cluster flags after correction. For all graphs: on the left, the NE façade; and on the right, the SW façade.

Table 3
Linear regression analysis results, the adjusted R^2 is provided for each couple of pyranometers.

Selected Clear Sky Days	NE1-NE2	NE1-NE3	NE2-NE3	SW1-SW2	SW1-SW3	SW2-SW3
5-May-2023	0.998	0.998	1.000	0.997	0.925	0.928
29-May-2023	0.992	0.997	0.997	0.998	0.992	0.995
5-Jun-2023	0.999	1.000	0.999	0.915	0.913	0.999
25-Jun-2023	0.997	1.000	0.997	0.928	0.924	0.999

pyranometer measurements with $QF_{night} = 0$ and $QF_{prec} = 1$ could be selected and analyzed to better understand the soiling phenomenon on pyranometers (i.e., rain can contribute to the deposition of soil, but also to the cleaning of the pyranometers' glass depending on the content of raindrops).

Shadow detection. The number of data points labeled as "*shaded*" ($QF_{shad} = 1$) and "*unshaded*" ($QF_{shad} = 0$) are presented for each pyranometer in Table 7.

The implemented shadow detection method permitted the identification of periodic shadows as visualized in Fig. 11. Two different clusters of shadows can be outlined: (i) the shadow from the opposite line of buildings, and (ii) the one from the same façade where the pyranometers are installed. In the NE pyranometers, the former is generally observed during the morning hours (solar azimuth angles between 50° to 120° and elevation lower than 30°), while the latter mostly occurs from the middle till the end of the day (solar azimuth angles between 125° to 310° and elevation lower than 60°). The opposite pattern (i.e., shadows from the monitored façade during the morning hours and shadows from surroundings from the middle till the end of the day) characterizes the SW façade. Therefore, the pyranometers applied to the NE façade were shaded for most of the monitoring time (circa 85% of the daytime hours), while the ones on the SW façade were shaded for circa 63% of the daytime hours (Table 7). During a typical clear sky day, the transition from shaded to unshaded conditions was observed firstly on the third floor's pyranometers (for both NE and SW facades). As the sun rises behind the building across the street canyon, the third floor receives direct solar irradiance, thereby the switch from shaded to unshaded typically starts earlier than on the lower floors. Indeed, the number of data points affected by periodic shading on the third floor is the lowest for both facades (55% for the SW façade, 85% for the NE façade).

Among the possible applications of the assigned QF_{shad} values, these

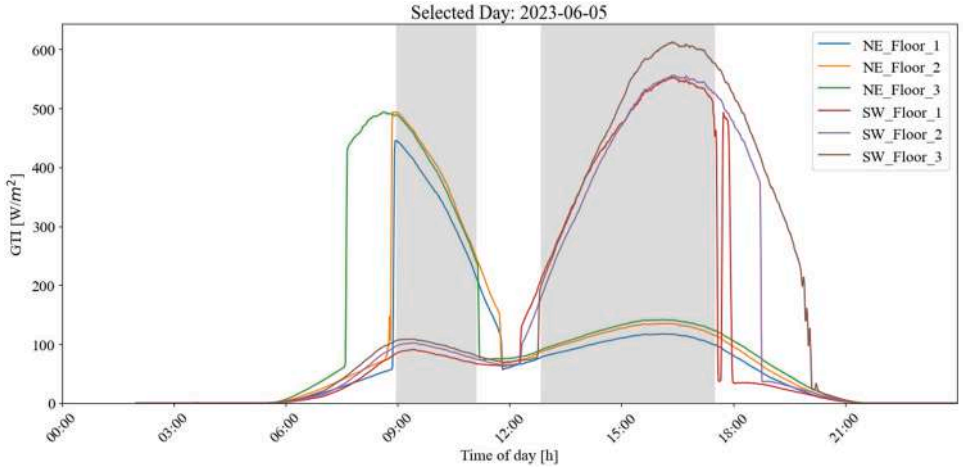

Fig. 9. Pyranometer measurements used in the linear regression analysis (grey area) for the 5th of June 2023.

Table 4
Quality flags of nighttime for the annual basis period for all the monitored pyranometers installed on both the NE and the SW facades.

Quality flag	Flag values	Flagged data points (number, [%])
QF_{night}	0	266 923 [51]
	1	255 797 [49]

can be used to select relatively high irradiance measurements that are collected when the pyranometers are shadowed. Such filtering represents the preliminary step in the investigation of diffuse solar irradiance contribution to façade solar energy potential as well as in the analysis of solar inter-building and ground reflections within the built environment.

5.3. Inter-sensor quality check

Consistency check. The consistency check resulted in about 0.5% (0.433%) of the daytime observations being labeled as incomplete due to at least one missing value. The flagged data points corresponded to data points in which the GHI range limit test was inapplicable (673 data points), along with 326 and 709 missing values from the temperature and DHI sensor, respectively. The number of data points flagged for

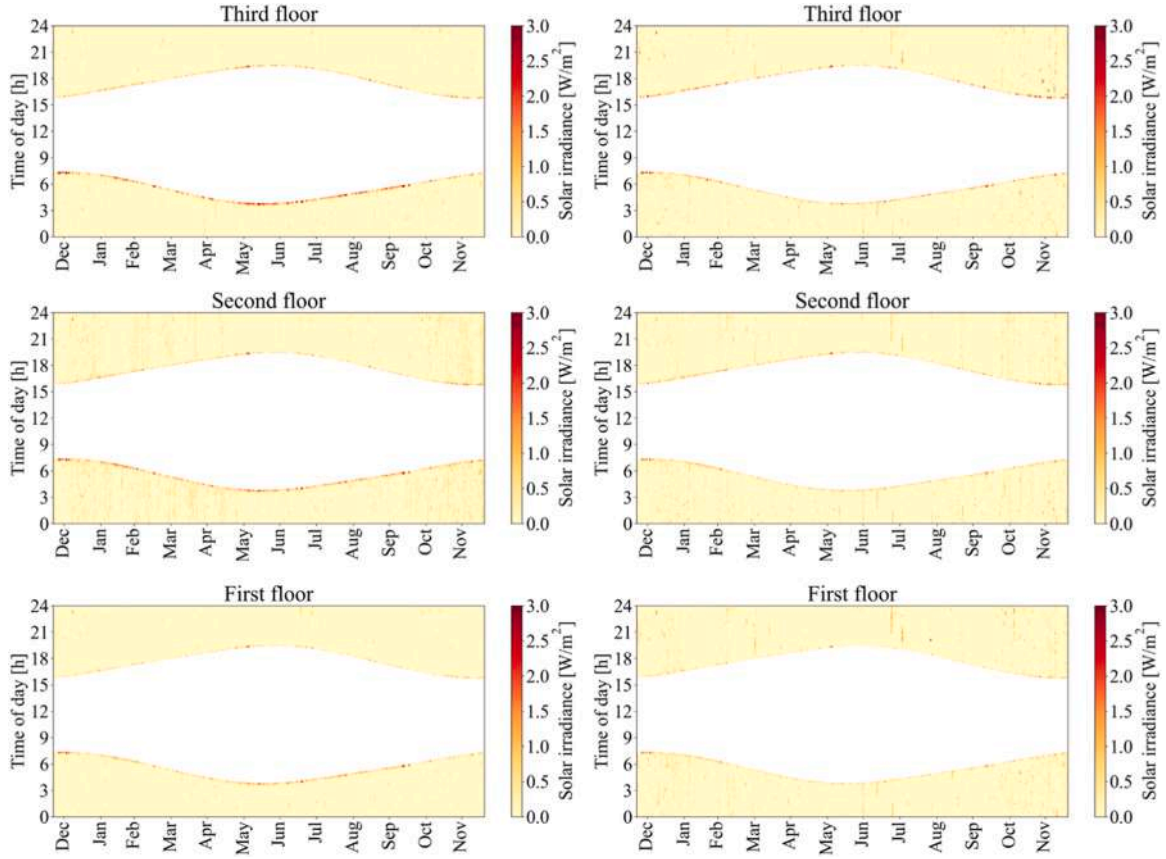

Fig. 10. Façade pyranometer readings flagged as nighttime for all the floors of the two analyzed facades: on the left, the NE façade; and on the right, the SW façade.

Table 5
Range limit test results for the HEPIA weather station and all pyranometers installed on both NE and SW facades. The analyzed data points only concern daytime observations ($QF_{night} = 0$).

Parameters	No test	Upper	Lower	Max. step
GHI_weather station	673	0	152	0
GTI_NE_1	0	3	3049	0
GTI_NE_2	0	7	1849	0
GTI_NE_3	0	9	1548	0
GTI_SW_1	0	0	3362	0
GTI_SW_2	0	0	2142	0
GTI_SW_3	0	3	1483	0

Table 6
Resulting flags of precipitation check for all pyranometers installed on both NE and SW facades. The analyzed data points only concern daytime observations ($QF_{night} = 0$).

Quality flag	Flag values	Flagged data points (number, [%])
QF_{prec}	0	264 794 [99.2]
	1	2129 [0.8]

Table 7
Number of data points flagged as "*shaded*" and "*unshaded*" for all pyranometers installed on both NE and SW facades. The analyzed data points only concern daytime observations ($QF_{night} = 0$).

Sensor location	$QF_{shad} = 0$ (number, [%])	$QF_{shad} = 1$ (number, [%])
1st Floor NE	34 801 [13]	232 122 [87]
2nd Floor NE	39 503 [14.4]	227 870 [85.4]
3rd Floor NE	40 305 [15]	226 618 [85]
1st Floor SW	81 236 [30.5]	185 687 [69.5]
2nd Floor SW	96 936 [36.3]	169 987 [63.7]
3rd Floor SW	118 702 [44.5]	148 221 [55.5]

consistency check is presented in Table 8.

5.4. Summary of the quality flags

The five QFs assigned during the QCS were combined into a single dataset for each pyranometer, which is represented in Fig. 12. The visual inspection of these heatmaps permitted to carry out the following considerations about the various QCs:

- Only a small number of data points managed to go through every QC without being flagged with a value different from the zero (yellow-colored data points in Fig. 12).
- The nighttime check (QF_{night}) and the shadow detection process (QF_{shad}) represented the QCs that assigned the highest number of flags with a value different than zero.
- Datapoints that failed the range limit tests ($QF_{range} > 0$) occurred within the same day (sequences of vertically aligned red-colored data points), thereby possibly indicating a temporary malfunctioning of the pyranometers.

5.5. Validation and further improvements of shadow detection

To validate the shadow detection algorithm, the GTI measurements have been compared with QFs assigned during the shadow detection. A period of six consecutive clear sky days ($k_{csi} > 0.8$), from June the 2nd to June the 7th, was considered so the occurrence of permanent shadow is more evident (Fig. 13). The visual comparison of the assigned QF_{shad} and GTI measurements (Fig. 13) permitted to verify the overall reliability of the developed shadow detection algorithm.

Nonetheless, this algorithm presented some limitations particularly in scenarios involving (i) instantaneous variations of solar irradiance and (ii) solar inter-building reflections. Several factors made challenging the clustering process such as:

- Persistence (after the preliminary filtering and smoothing steps) of data points characterized by temporary shadows that occurred during clear sky days (e.g., shadow from birds or isolated clouds) as well as by increases in solar irradiance due to solar reflections from surroundings and cloud enhancement effects. These outliers created a disturbance, especially during partly overcast days, and need to be excluded from the clustering through more accurate outlier detection techniques. In this regard, the statistical approach proposed by Castillejo-Cuberos and Escobar [23] for detecting cloud enhancement events can represent an adequate tool to integrate into the hereby presented shadow detection algorithm.
- The smoothing technique can be improved as demonstrated by the data points with low solar irradiance values that were generated (see Fig. 14). The ideal outcome would be a gradual transition of GTI values (unobstructed observations) between two clear-cut significantly low measurements (permanently obstructed measurements). Smoothing techniques based on graphical noise reduction may offer better performance and outcomes as clustering inputs compared to the rolling window smoothing technique. However, graphical noise reduction would be computationally expensive and might overlook spatial data distribution.
- K-means clustering is sensitive to outliers and density variations within the cluster, both of which exist in the utilized datasets (bell-shaped). Indeed, the k-means clustering is usually applied to data that is well-separated into spherical clusters and similar variance within each cluster. Considering the non-spherical nature of the clusters of this study, alternative clustering techniques such as density-based spatial clustering and hierarchical clustering or applications with noise reduction may allow further refinement of the results. However, these techniques need a higher computational time, thus limiting their application in similar studies.
- Another limitation concerns the local outlier detection algorithm that failed whenever some misclustered data points were excessively close in the α-ε plane. Consequently, the algorithm failed to recognize these data points as outliers. This limitation can be overcome by adjusting the number of neighborhoods checked for outliers or by manually focusing on problematic areas to enhance the detection and correction process.

5.6. Limitations of the study

In this section, the main limitations of the study are discussed along with their implications.

Firstly, the weather station is not located in the Rue des Grottes avenue, but in the proximity (circa 300 m distance). As one-minute resolution data were used, even a similarly short distance is enough for having different irradiance conditions (influenced by local cloud patterns), particularly during overcast days. However, the distance from the monitored street canyon was not significant enough to justify preferring GHI data retrieved from satellite observations or numerical reanalysis instead of ground measurements, which are typically provided with a spatial resolution of 9 km.

A second limitation is related to the presence of a retractable sun awning installed near the pyranometer on top of the shop located on the ground floor of the SW façade. When the sun awning was open (i.e., pulled outside), it possibly increased the solar irradiance reflected towards the pyranometer, hence resulting in higher readings. Although there is a lack of information concerning when the sun awning was open, it may be assumed that this occurred during the commercial activity's operating hours. Thus, such a limitation should be considered when analyzing the data, particularly when investigating solar reflections

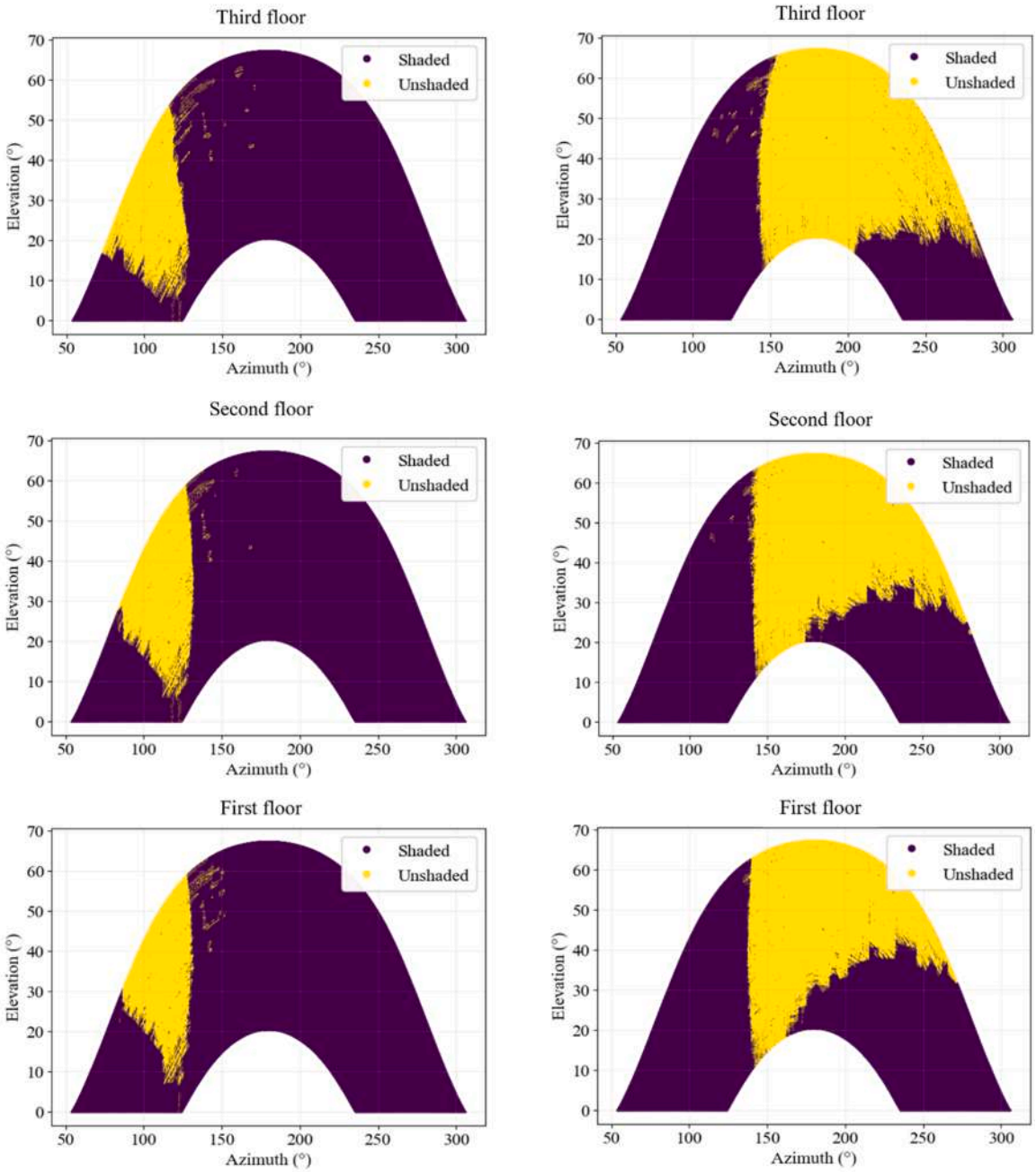

Fig. 11. Shadow detection results for all the pyranometers installed on the two analyzed facades: the NE façade on the left, and the SW façade on the right.

Table 8
Data points flagged for consistency check for all pyranometers installed on both NE and SW facades. The analyzed data points only concern daytime observations ($QF_{night} = 0$).

Quality flag	Flag values	Flagged data points (number, [%])
QF_{cons}	0	265 768 [99.5]
	1	1155 [0.5]

within the street canyon.

Additionally, various data sources were exploited in this study, as described in Section 3.3. In this regard, satellite observations from CAMS were used to retrieve information about the GHI_{csky} and the GHI_{extra}. Since ground measurements of the atmosphere and its composition were not available for the chosen location, gridded data based on geostationary satellites were used. Furthermore, certain steps of the proposed QCS are constrained by data availability. For instance, the precipitation check could not be performed if the precipitation data was unavailable. Similarly, if the GTI measurements were obtained from a single pyranometer, it was impossible to perform the alignment check. This limitation highlighted the importance of comprehensive data availability for the proposed QCS.

Finally, although this limitation did not affect the present study, the orientation check can only function if data from extremely clear sky days are provided. Issues may arise whenever measurements cover a short time interval, mostly representative of overcast conditions. Therefore, including additional environmental data (e.g., cloud cover, clearness index, diffuse fraction) and exploiting more sophisticated statistical techniques (e.g., time-series analysis, Granger causality test, machine learning) represent two strategies to enhance the orientation check.

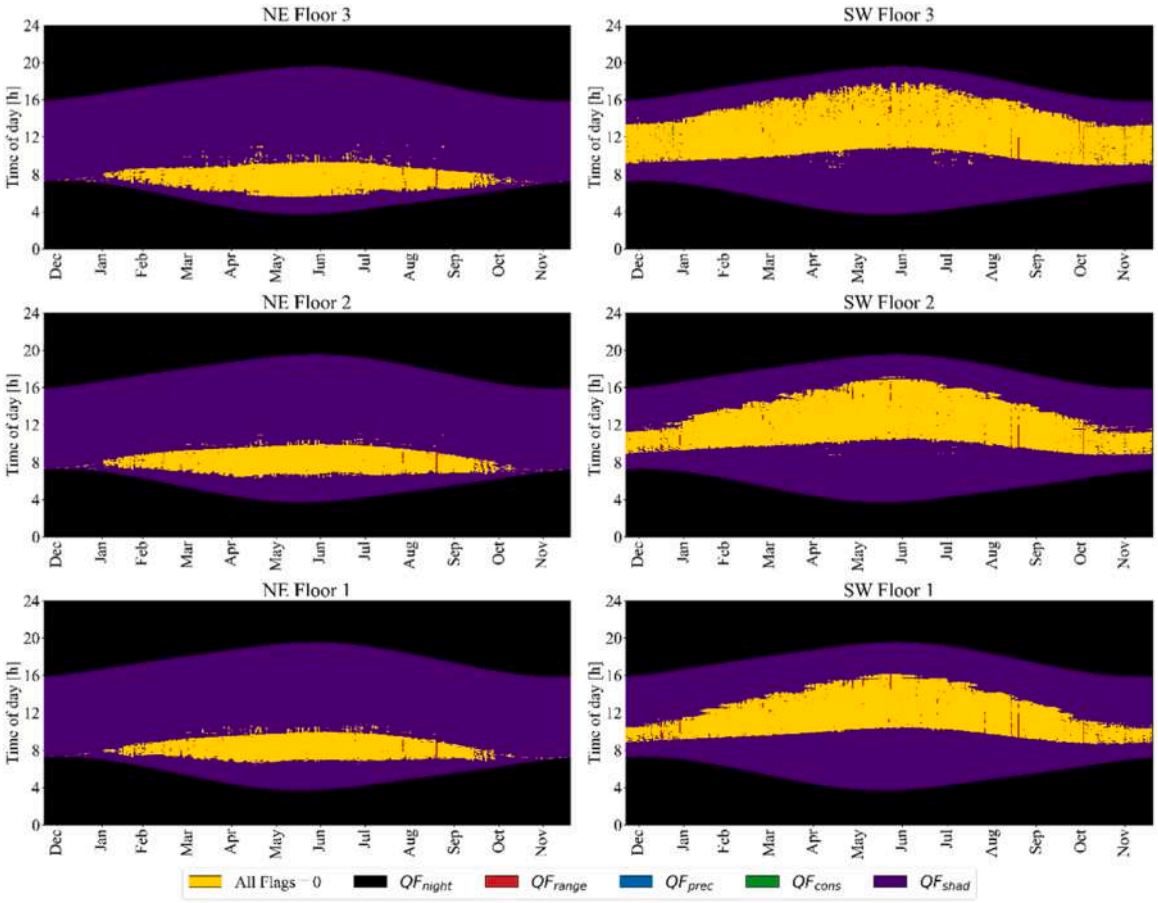

Fig. 12. Overview of the QFs assigned to each data point. It is worth noting that the shown QF referred to the first QC that was not passed. For example, if the data point failed both the nighttime check and the range limit tests, only QF_{night} is shown in the graph.

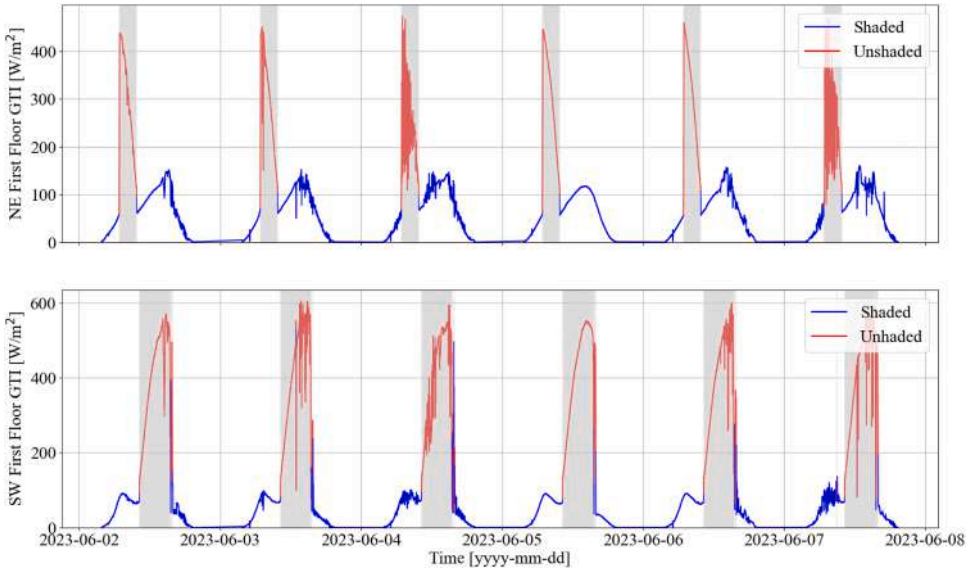

Fig. 13. GTI measurements for the first floor of NE and SW facades. Data points flagged "*unshaded*" are indicated by the red line and highlighted with a grey background, while data points flagged "*shaded*" are represented with a blue line.

6. Conclusions and future work

This study introduces a QCS for solar irradiance measurements on facades, demonstrated through a case study in a typical urban street canyon in Geneva. This QCS addresses the challenges of the urban built environment, such as the influence of shadows on pyranometer readings. Five QCs were defined to identify the potential flaws and disturbances in the dataset so that these data points could be flagged accordingly.

Regarding the application of the QCS to measurements from Rue des

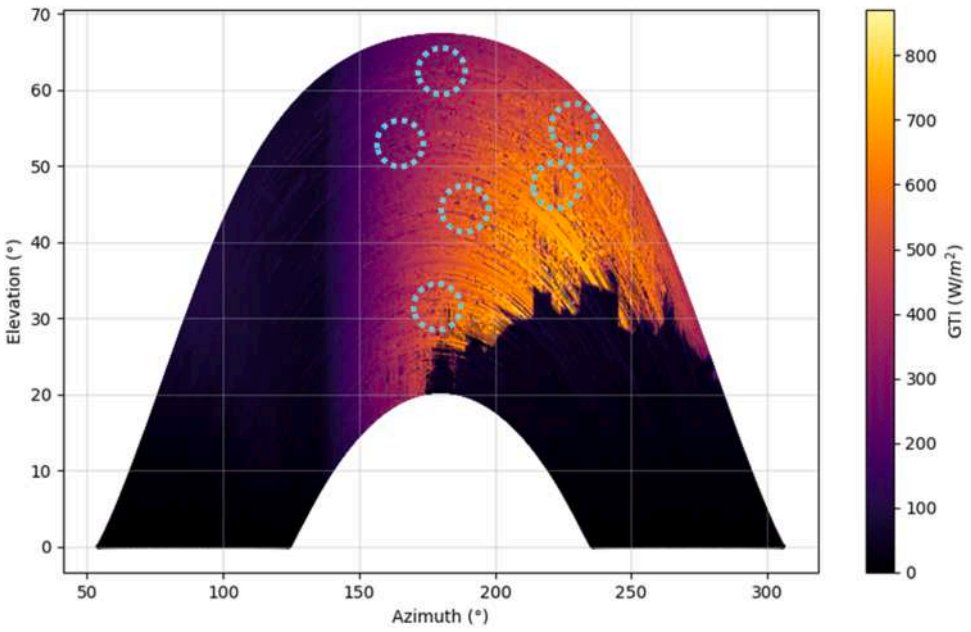

Fig. 14. Misestimated data points circles with blue dots after the smoothing process. Measurements are retrieved from the pyranometer installed on the SW façade, second floor.

Grottes, this study highlighted the minimum effect (i.e., low number of flagged data points) of the range limit tests, along with the precipitation and consistency checks. Conversely, periodic shadow detection played an important role in the flagging process.

The main findings of this study are:

- A quality control scheme for global tilted irradiance measured in an urban street canyon.
- A fully automated, statistically informed approach eliminating the need for manual flagging.
- An algorithm for the detection of periodic shadows, incorporating clustering cascade and local outlier detection.

Moreover, the quality flags assigned throughout the different QCs enabled the identification and exclusion of erroneous data, thereby improving the accuracy of the dataset for future validation studies. Indeed, results contribute to establishing a robust foundation for the validation of a new functionality of the Grand Geneva Solar Cadaster allowing the estimation of solar irradiance on vertical surfaces. Thus, the proposed QCS establishes a benchmark for the preparation of datasets to validate digital tools for solar analysis in urban environments.

Among the future developments of this study, the improvement of the clustering process should be prioritized to better detect periodic shadows. In this regard, a more refined checking of the instantaneous variations among the measurements at the cluster boundaries after each clustering iteration could enhance the accuracy and reliability of the shadow detection method. Additionally, a new quality flag could be introduced to label data points characterized by solar reflections from the ground and surrounding buildings. The clustering cascade could be used to identify these solar reflections events similarly to its application in the shadow detection algorithm.

CRediT authorship contribution statement

Nesrin Irmak Köker: Writing – original draft, Visualization, Methodology, Formal analysis, Data curation, Conceptualization. **Martina Giorio:** Writing – review & editing, Methodology, Conceptualization. **Gabriele Lobaccaro:** Writing – review & editing, Visualization, Supervision, Project administration, Funding acquisition. **Gilles Desthieux:** Writing – review & editing, Resources, Funding acquisition. **Peter Gallinelli:** Writing – review & editing, Formal analysis, Data curation. **Bjørn Petter Jelle:** Project administration, Funding acquisition, Supervision, Writing – review & editing. **Mattia Manni:** Writing – review & editing, Writing – original draft, Visualization, Supervision, Methodology, Conceptualization.

Declaration of competing interests

The authors declare that they have no known competing financial interests or personal relationships that could have appeared to influence the work reported in this paper.

Acknowledgments

The authors acknowledge the support from the Research Council of Norway and various partners through the research project “Enhancing Optimal Exploitation of Solar Energy in Nordic Cities through the Digitalization of the Built Environment” (Helios, project no. 324243) and from the European Commission through the research project “An Open Innovation Ecosystem for Exploitation of Materials for Building Envelopes towards Zero Energy Buildings” (Exploit4InnoMat, project no, 101092339). The monitoring system with pyranometers was installed in Geneva thanks to the financing of the University of Applied Sciences of Western Switzerland (HES-SO) and the Geneva Energy Service (SIG) in the framework of the VALES project.

References

[1] International renewable energy agency, world energy transition - outlook 2022: 1.5 °C pathway, Abu Dhabi, 2022. https://irena.org/energytransition.
[2] United Nations, world cities report 2022: envisaging the future of cities, 2022. https://unhabitat.org/sites/default/files/2022/06/wcr_2022.pdf.
[3] C. Lindkvist, E. Juhasz-Nagy, B.F. Nielsen, H.M. Neumann, G. Lobaccaro, A. Wyckmans, Intermediaries for knowledge transfer in integrated energy planning of urban districts, Technol. Forecast. Soc. Change. 142 (2019) 354–363, https://doi.org/10.1016/J.TECHFORE.2018.07.020.
[4] G. Desthieux, C. Carneiro, A. Susini, N. Abdennadher, A. Boulmier, A. Dubois, R. Camponovo, D. Beni, M. Bach, P. Leverington, E. Morello, Solar Cadaster of Geneva: A Decision Support System For Sustainable Energy Management BT - From Science to Society, in: B. Otjacques, P. Hitzelberger, S. Naumann, V. Wohlgemuth (Eds.), Springer International Publishing, Cham, 2018: pp. 129–137.

[5] T. Santos, N. Gomes, S. Freire, M.C. Brito, L. Santos, J.A. Tenedório, Applications of solar mapping in the urban environment, Appl. Geogr. 51 (2014) 48–57.
[6] K. Bódis, I. Kougias, A. Jäger-Waldau, N. Taylor, S. Szabó, A high-resolution geospatial assessment of the rooftop solar photovoltaic potential in the European Union, Renew. Sustain. Energy Rev. 114 (2019) 109309, https://doi.org/10.1016/j.rser.2019.109309.
[7] M. Manni, E. Bonamente, G. Lobaccaro, F. Goia, A. Nicolini, E. Bozonnet, F. Rossi, Development and validation of a monte carlo-based numerical model for solar analyses in urban canyon configurations, Build. Environ. 170 (2020) 106638, https://doi.org/10.1016/J.BUILDENV.2019.106638.
[8] G. Desthieux, C. Carneiro, R. Camponovo, P. Ineichen, E. Morello, A. Boulmier, N. Abdennadher, S. Dervey, C. Ellert, Solar energy potential assessment on rooftops and facades in large built environments based on LiDAR data, image processing, and cloud computing. methodological background, application, and validation in Geneva (Solar cadaster), Front. Built Environ (2018) 4, https://doi.org/10.3389/fbuil.2018.00014.
[9] G. Desthieux, M. Thebault, Solar governance for the transborder agglomeration of the Greater Geneva based on the solar cadaster development, Front. Built Environ. 10 (2024), https://doi.org/10.3389/fbuil.2024.1347056.
[10] B. Raybaud, G. Desthieux, Adapted strategy for large-scale assessment of solar potential on facades in urban areas focusing on the reflection component, Sol. Energy Adv. 2 (2022) 100030, https://doi.org/10.1016/J.SEJA.2022.100030.
[11] B. Raybaud, Evaluation De L'impact Des Propriétés Optiques Large-Bande De L'environnement Sur Le Productible (énergie incidente) En Milieu Urbain, Université de Lyon, 2020.
[12] A. Ohmura, E.G. Dutton, B. Forgan, C. Fröhlich, H. Gilgen, H. Hegner, A. Heimo, G. König-Langlo, B. McArthur, G. Müller, R. Philipona, R. Pinker, C.H. Whitlock, K. Dehne, M. Wild, Baseline surface radiation network (BSRN/WCRP): new precision radiometry for climate research, Bull. Am. Meteorol. Soc 79 (1998) 2115–2136, https://doi.org/10.1175/1520-0477(1998)079. <2115:BSRNBW>2.0.CO;2.
[13] A. Roesch, M. Wild, A. Ohmura, E.G. Dutton, C.N. Long, T. Zhang, Assessment of BSRN radiation records for the computation of monthly means, Atmos. Meas. Tech. 4 (2011) 339–354, https://doi.org/10.5194/AMT-4-339-2011.
[14] R. Urraca, T. Huld, A.V. Lindfors, A. Riihelä, F.J. Martinez-de-Pison, A. Sanz-Garcia, Quantifying the amplified bias of PV system simulations due to uncertainties in solar radiation estimates, Sol. Energy. 176 (2018) 663–677, https://doi.org/10.1016/J.SOLENER.2018.10.065.
[15] E. Lorenz, P. Guthke, A. Dittmann, N. Holland, W. Herzberg, S. Karalus, B. Müller, C. Braun, W. Heydenreich, Y.M. Saint-Drenan, High resolution measurement network of global horizontal and tilted solar irradiance in southern Germany with a new quality control scheme, Sol. Energy. 231 (2022) 593–606, https://doi.org/10.1016/J.SOLENER.2021.11.023.
[16] D. Yang, G.M. Yagli, H. Quan, Quality control for solar irradiance data, in: 2018 IEEE Innov. Smart Grid Technol. - Asia (ISGT Asia), 2018, pp. 208–213, https://doi.org/10.1109/ISGT-Asia.2018.8467892.
[17] C.N. Long, Y. Shi, An automated quality assessment and control algorithm for surface radiation measurements, Open Atmos. Sci. J. 2 (2008) 23–37, https://doi.org/10.2174/1874282300802010023.
[18] M. Geiger, L. Diabaté, L. Ménard, L. Wald, A web service for controlling the quality of measurements of global solar irradiation, Sol. Energy. 73 (2002) 475–480, https://doi.org/10.1016/S0038-092X(02)00121-4.
[19] M. Journée, C. Bertrand, Quality control of solar radiation data within the RMIB solar measurements network, Sol. Energy. 85 (2011) 72–86, https://doi.org/10.1016/j.solener.2010.10.021.
[20] D. Perez-Astudillo, D. Bachour, L. Martin-Pomares, Improved quality control protocols on solar radiation measurements, Sol. Energy. 169 (2018) 425–433, https://doi.org/10.1016/j.solener.2018.05.028.
[21] R. Urraca, A. Sanz-Garcia, I. Sanz-Garcia, BQC: A free web service to quality control solar irradiance measurements across Europe, Sol. Energy. 211 (2020) 1–10, https://doi.org/10.1016/J.SOLENER.2020.09.055.
[22] B. Espinar, L. Wald, P. Blanc, C. Hoyer-Klick, M. Schroedter Homscheidt, T. Wanderer, Project ENDORSE - Excerpt of the report on the harmonization and qualification of meteorological data:Procedures for quality check of meteorological data, 2011. https://hal-mines-paristech.archives-ouvertes.fr/hal-01493608.
[23] A. Castillejo-Cuberos, R. Escobar, Detection and characterization of cloud enhancement events for solar irradiance using a model-independent, statistically-driven approach, Sol. Energy. 209 (2020) 547–567, https://doi.org/10.1016/j.solener.2020.09.046.